Solvent and ligand substitution effects on electrocatalytic reduction of CO2 with [Mo(CO)4(x,x′-dimethyl-2,2′-bipyridine)] (x = 4-6) enhanced at a gold cathodic surface

Article

Accepted Version

FUNDAMENTALS & APPLICATIONS

CHEMELECTROCHEM

ANALYSIS & CATALYSIS, BIO & NANO, ENERGY & MORE

Accepted Article

Title: Solvent and Ligand Substitution Effects on Electrocatalytic Reduction of CO2 with [Mo(CO)4(x,x′-dimethyl-2,2′-bipyridine)] (x = 4-6) Enhanced at a Gold Cathodic Surface

Authors: Frantisek Hartl, James O. Taylor, and Roisín D. Leavey

To be cited as: *ChemElectroChem* 10.1002/celc.201800879

Link to VoR: http://dx.doi.org/10.1002/celc.201800879

A Journal of

ChemPubSoc Europe

WILEY-VCH

www.chemelectrochem.org

WILEY-VCH

COMMUNICATION

Solvent and Ligand Substitution Effects on Electrocatalytic Reduction of CO_2 with [Mo(CO)$_4$(x,x'-dimethyl-2,2′-bipyridine)] (x = 4-6) Enhanced at a Gold Cathodic Surface

James O. Taylor[a], Roisín D. Leavey[a], and František Hartl*[a]

Abstract: A series of molybdenum tetracarbonyl complexes with dimethyl-substituted 2,2′-bipyridine (dmbipy) ligands were investigated by cyclic voltammetry (CV) combined with infra-red spectroelectrochemistry (IR-SEC) in tetrahydrofuran (THF) and *N*-methyl-2-pyrrolidone (NMP) to explore their potential in a reduced state to trigger electrocatalytic CO_2 reduction to CO. Addressed is their ability to take advantage of a low-energy, CO-dissociation two-electron ECE pathway available only at an Au cathode. A comparison is made with the reference complex bearing unsubstituted 2,2'-bipyridine (bipy). The methyl substitution in the 6,6'-positions has a large positive impact on the catalytic efficiency. This behaviour is ascribed to the advantageous positioning of the steric bulk of the methyl groups, which further facilitates CO dissociation from the 1e$^-$ reduced parent radical anion. In the contrary, the substitution in the 4,4′-positions appears to have a negative impact on the catalytic performance, exerting a strong stabilizing effect on the π-accepting CO ligands and, in THF, preventing exploitation of the low-energy dissociative pathway.

Dwindling fossil fuel reserves and mounting yearly average temperatures has continued to drive the increasingly urgent need to develop renewable technologies. Despite this, continuing research efforts to produce commercially viable functionalization of CO_2 remains some distance away.[1–4] Currently, much of the literature regarding molecular electrochemical activation of CO_2 still continues to explore the catalytic properties of the heavier members of Group-7 (Re[5–10]), Group-8 (Ru[11–18] and Os[19–21]) and Group-9 (Rh[22,23] and Ir[24–27]) triads. These "first-generation" electrocatalysts must be phased out; encouragingly, cheaper alternatives exist within the same groups – Mn[28–36] substituting Re, Fe[37–45] substituting Ru and Os, and Co substituting Rh and Ir.[46–48] However, the community's focus on late transition metals is leaving the Group-6 metals (Cr, Mo, W) rather neglected, despite the high potential for the comparatively abundant metal triad to function as both high-performance alternatives to the noble metals and photostable alternatives to the hot-topic manganese carbonyls.[49–52]. Indeed, two recent reviews of homogenous molecular catalysts highlighted this under-representation of Group-6 complexes.[53,54] Attention is often paid to the Re-tricarbonyl motif, which since the first accounts by Lehn et al.[55] has proven a robust platform from which to analyze electrocatalytic effects of a range of non-innocent α-diimine ligands.[1] Beside the emerging tetracarbonyl α-diimine catalyst precursors discussed hereinafter, complexes of the type [Mo(η^3-allyl)(CO)$_2$(α-diimine)X] (X = pseudo-halide) are another notable family among Group-6 carbonyls, which also involve catalytically active species along their reduction path.[56,57] Complexes [M(CO)$_4$(bipy)] exhibit a relatively simple cathodic pathway (Scheme 1). In the primary step, they undergo reversible 1e$^-$ reduction at R1/O1, forming a stable 6-coordinate radical anion, [M(CO)$_4$(bipy)]$^{\bullet-}$. The radical anion is subsequently reduced by 1e$^-$ at R2, which is accompanied by rapid CO dissociation in an irreversible EC step to yield the 5-coordinate dianion, [M(CO)$_3$(bipy)]$^{2-}$. On the reverse scan only the oxidation of this electron-rich species to short-lived [M(CO)$_3$(bipy)]$^{\bullet-}$ is seen at O2', followed by rapid CO re-coordination and recovery of the tetracarbonyl radical anion. Recent work in our group[49] has shown that at a gold cathode the onset of the catalytic wave corresponding to CO_2 reduction by [M(CO)$_3$(bipy)]$^{2-}$ can be much less negative than at R2, especially in NMP. The onset of a catalytic wave now occurs at R2', corresponding to the concomitant reduction of the transient [M(CO)$_3$(bipy)]$^{\bullet-}$ to the 2e$^-$ reduced catalyst [M(CO)$_3$(bipy)]$^{2-}$, that occurs almost 600 mV less negative than on a platinum electrode. Unlike the latter cathodic material, the gold surface is promoting dissociation of CO from [M(CO)$_4$(bipy)]$^{\bullet-}$. This mechanism has recently been confirmed by Cowan and co-workers using SFG spectroscopy.[58] SFG is a relatively new, complex technique that involves exposing the sample at the surface of the electrode to both infrared and UV-light beams and collecting the resulting VSFG signal, in this case due to catalytically active [Mo(CO)$_3$(bipy)]$^{2-}$ and its protonated form, [M(CO)$_3$(bipy-H)]$^-$, before the onset of the second cathodic wave R2 corresponding to the reduction of [M(CO)$_4$(bipy)]$^{\bullet-}$ specifically adsorbed at the gold electrode surface. The best catalytic performance in this respect was seen[49] with CV and IR-SEC when the gold electrode was combined with the NMP electrolyte. It is likely that NMP is also aiding the carbonyl dissociation in the singly reduced state. Hereinafter, this study is extended to encompass the three dimethylated bipy derivatives of the title compound, the goal being to ascertain (i) whether this low-energy catalytic pathway can be considered a general feature of [Mo(CO)$_4$(x,x'-dmbipy)] (x,x'-dmbipy = x,x'-dimethyl-2,2'-bipyridine, x = 4-6) complexes, and (ii) what impact varying the position of the methyl groups at bipy has on the catalyst's ability to access the low-energy ECE pathway.

[a] Professor František Hartl, James O. Taylor, Roisin H. Leavey
School of Chemistry, Food and Pharmacy, Department of Chemistry
University of Reading, Whiteknights Campus, Reading, RG6 6AD
E-mail: f.hartl@reading.ac.uk

Supporting information for this article is given via a link at the end of the document.

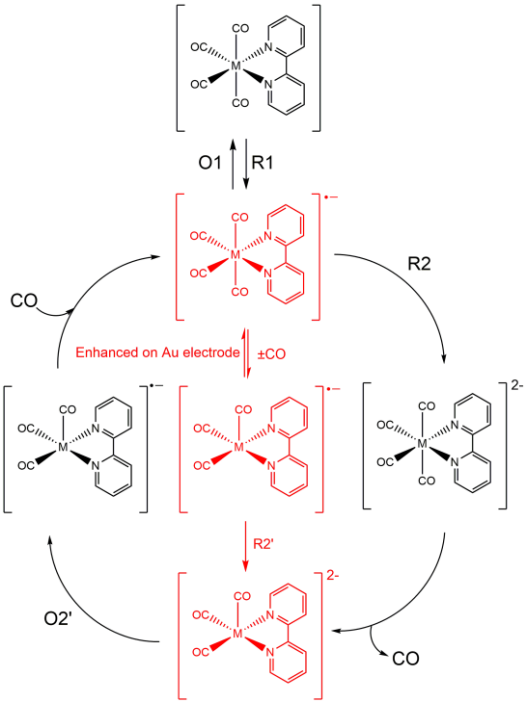

Scheme 1. Electrochemical reduction pathways of the complexes $[M(CO)_4(bipy)]$ (M = Cr, Mo, W), and reoxidation of $[M(CO)_3(bipy)]^{2-}$. Highlighted in red is the alternate low-energy ECE cathodic pathway producing the active catalytic species, $[M(CO)_3(bipy)]^{2-}$, ca. 600 mV less negatively. This pathway can be easily accessed by using a gold electrode, which is enhancing the dissociation of CO from the specifically adsorbed parent tetracarbonyl radical anion.

Table 1. Electrode potentials of $[Mo(CO)_4(x,x'\text{-dmbipy})]$ (x = 4-6) and their reduction products in THF/Bu_4NPF_6 using a Pt disc microelectrode.

Redox Step	*E* / V vs Fc/Fc^+		
	x = 4	x = 5	x = 6
$[Mo(CO)_4(dmbipy)] \leftrightarrow [Mo(CO)_4(dmbipy)]^{\bullet-}$ (R1)	-2.15 [a]	-2.19 [a]	-2.13 [a]
$[Mo(CO)_4(dmbipy)]^{\bullet-} \leftrightarrow [Mo(CO)_4(dmbipy)]^{2-}$ (R2)	-2.67 [b]	-2.74 [b]	-2.71 [b]
$[Mo(CO)_3(dmbipy)]^{2-} \leftrightarrow [Mo(CO)_3(dmbipy)]^{\bullet-}$ (O2')	-2.39 [c]	-2.36 [c]	-2.41 [c]

[a] $E_{1/2}$ values. [b] $E_{p,c}$ values. [c] $E_{p,a}$ values. Potentials for $[Mo(CO)_4(bipy)]$ are: R1: -2.07 V ($E_{1/2}$), R2: -2.73 V ($E_{p,c}$) and O2': -2.32 V ($E_{p,a}$).[49]

Cyclic voltammetry (CV) with $[Mo(CO)_4(x,x'\text{-dmbipy})]$ was first conducted in argon-saturated THF, at a Pt (Figure 1) and Au (Figure S1) microdisc. The CV responses indicate that quite expectedly all three dmbipy complexes under study follow the general pathway laid out in Scheme 1. The methyl groups shift the cathodic potential R1 more negatively by 60-120 mV compared to the reduction of the 2,2'-bipyridine ligand.[49] This can be attributed to the electron donating effect of the methyl substituents rising the LUMO (bipy) energy. A comparable shift is reported for $[Re(CO)_3(x,x'\text{-dmbipy})Cl]$ (x = 3 and 5) vs $[Re(CO)_3(bipy)Cl]$.[59] The formation of the π-delocalized 5-coordinate dianion, $[Mo(CO)_3(x,x'\text{-dmbipy})]^{2-}$, in the THF electrolyte at R2 is hardly affected, Tables 1 (Pt) and S1 (Au). From these observations we can infer that migration of the methyl sites at bipy in $[Mo(CO)_4(x,x'\text{-dmbipy})]$ has only a limited electronic effect on the LUMO of the parent complex and stability of the tetracarbonyl radical anion in solution.

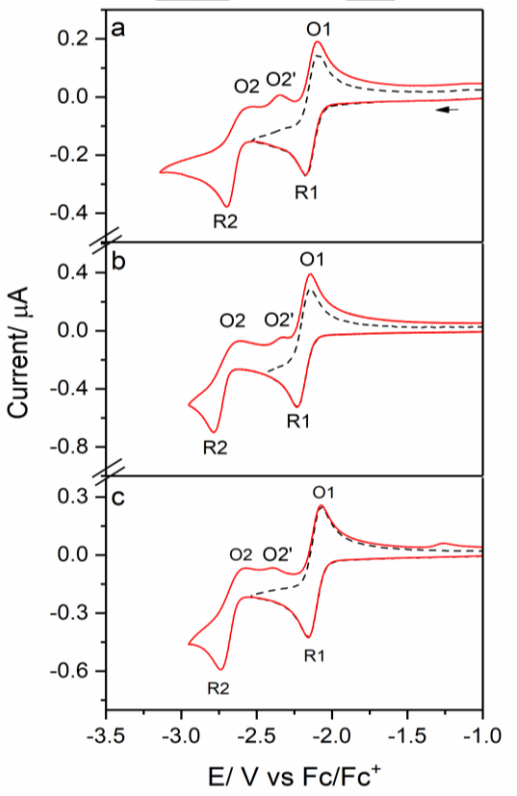

Figure 1. CV of $[Mo(CO)_4(x,x'\text{-dmbipy})]$ in argon-saturated THF/Bu_4NPF_6. (a) x = 4. (b) x = 5. (c) x = 6. Scan rate: 100 mV s^{-1}. Pt disc microelectrode. The arrow indicates the initial scan direction.

The analysis of the cathodic behaviour of $[Mo(CO)_4(x,x'\text{-dmbipy})]$ in NMP/Bu_4NPF_6 by cyclic voltammetry at ambient conditions (Figure S2 and Table S2 at a Pt microdisc, and Figure S3 and Table S3 at an Au microdisc) leads to a similar description as in THF, with the following notable differences observed. First, the parent reduction potentials (R1) are slightly less negative (130 – 150 mV) in NMP than in THF. Second, the cathodic wave R2', belonging to the reduction of $[M(CO)_3(x,x'\text{-dmbipy})]^{\bullet-}$, was detectable at the Au microdisc cathode on the forward cathodic scan beyond R1 for x = 4 and 5 (Figure S3 (a-b)). The CO dissociation from $[M(CO)_4(x,x'\text{-dmbipy})]^{\bullet-}$, responsible for the appearance of R2', is apparently most pronounced under these conditions, in agreement with the strong electrocatalytic performance in NMP at a gold electrode surface (see below). Third, the 5-coordinate complex $[Mo(CO)_3(x,x'\text{-dmbipy})]^{2-}$ is not the only two-electron-reduced species (formed at R2 and R2') detectable by cyclic voltammetry due to its anodic response at O2'. The continued reverse anodic scan starting beyond R2 reveals the O1/R1 peak-current ratio to depart from unity more

than in THF, especially for x = 4 and 6. A new anodic wave is seen between -1 and -1.2 V (Pt) and between -1.2 and -1.5 V (Au). Combined with IR spectroelectrochemistry (see below), the most likely assignment of this anodic wave is the oxidation of the stabilized protonated dianion keeping the tetracarbonyl coordination even after the two-electron reduction, $[Mo(CO)_4(x,x'\text{-dmbipy-H})]^-$, which appears to be the main ultimate reduction product in NMP, formed on a timescale of a few seconds.

Using a platinum working microelectrode in CO_2-saturated THF, the cathodic wave R1 was passed without any evidence for the significant current growth that is usually associated with catalytic CO_2 reduction. Under these conditions, a behaviour comparable to that of $[Mo(CO)_4(bipy)]$ (reproduced here in Figures S4 and S5)[49] was observed. The onset of the catalytic wave is not seen until the second reduction at R2 is passed (Figure 2), producing the 5-coordinate dianion $[Mo(CO)_3(x,x'\text{-dmbipy})]^{2-}$ exclusively from the corresponding unstable tetracarbonyl dianion (the EEC path). The most active species towards CO_2 in the series proves to be $[Mo(CO)_3(6,6'\text{-dmbipy})]^{2-}$, showing the highest catalytic current.

The catalytic performance in THF/CO_2 becomes generally enhanced at the gold disc microelectrode (Figure 3). Again, R1 is passed without any obvious change compared to the reversible behavior under argon. For $[Mo(CO)_4(x,x'\text{-dmbipy})]$ (x = 4 and 5), the catalytic wave remains largely associated with R2, but the catalytic activity is higher compared to that at the Pt microdisc. Only $[Mo(CO)_4(6,6'\text{-dmbipy})]$ shows the expected[49] shift of the catalytic wave to less negative potentials, close to the theoretical R2' wave associated with O2' (Figure 1). Apparently, in THF, the bipy substitution in the 4,4'- and 5,5'-positions is hindering the alternate low-energy pathway, presumably by strengthening Mo–CO bonds and moving the equilibrium toward the 6-coordinate radical anion, $[Mo(CO)_4(x,x'\text{-dmbipy})]^{\bullet-}$. The methyl substituents in the 6,6'-positions adjacent to the Mo-NCCN metallacycle may facilitate CO dissociation from the latter radical anion and shift the equilibrium toward the concomitantly reducible transient $[Mo(CO)_3(6,6'\text{-dmbipy})]^{\bullet-}$ both on steric and electronic grounds, likely driven by increased stabilizing delocalization of the added electron density over the metallacycle in the 5-coordinate geometry.[60] Indeed, $[Mo(CO)_4(6,6'\text{-dmbipy})]$ responds less negatively, showing significant enhancement of the current directly behind R1, to the gold cathode than even the reference complex $[Mo(CO)_4(bipy)]$ (Figures 3c and S5(a)).

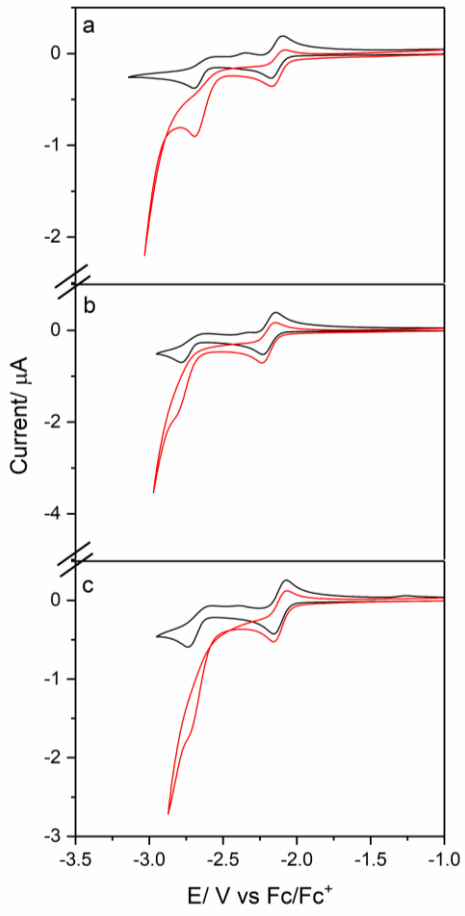

Figure 2. CV of $[Mo(CO)_4(x,x'\text{-dmbipy})]$ in CO_2-saturated THF/Bu_4NPF_6. (a) x = 4. (b) x = 5. (c) x = 6. Scan rate: 100 mV s^{-1}. Black curves - under argon, red curves - under CO_2. Pt disc microelectrode.

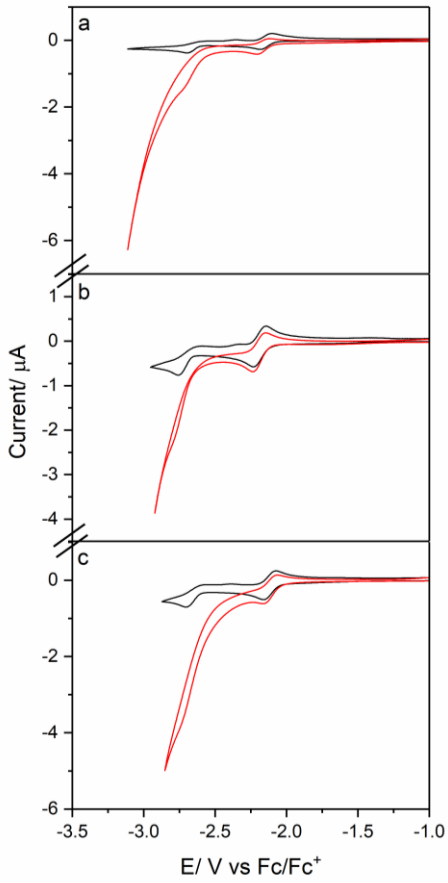

Figure 3. CV of $[Mo(CO)_4(x,x'\text{-dmbipy})]$ in CO_2-saturated THF/Bu_4NPF_6. (a) x = 4. (b) x = 5. (c) x = 6. Scan rate: 100 mV s^{-1}. Black curves - under argon, red curves - under CO_2. Au disc microelectrode.

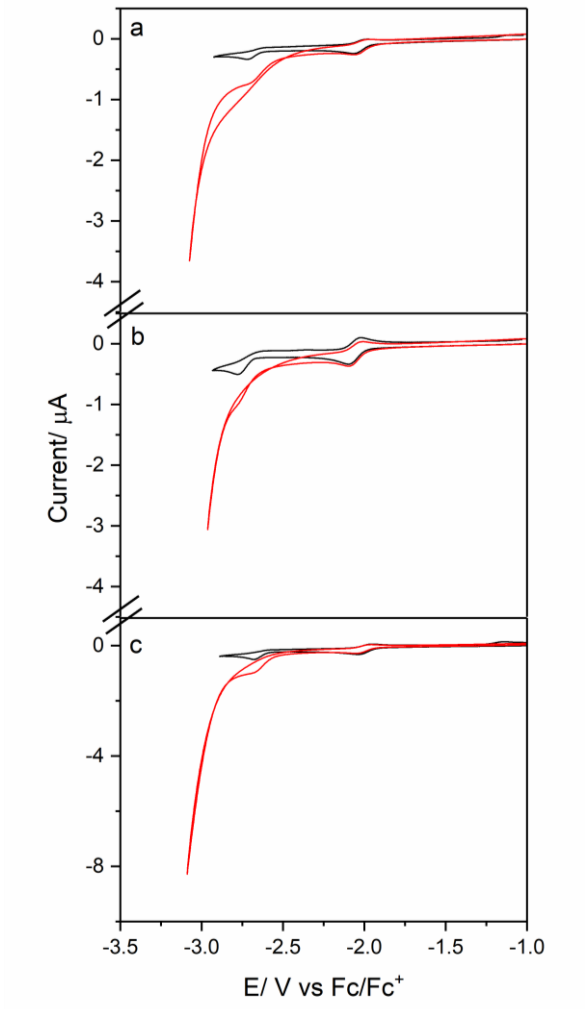

Figure 4. CV of $[Mo(CO)_4(x,x'\text{-dmbipy})]$ in CO_2-saturated NMP/Bu_4NPF_6. (a) x = 4 (b) x = 5. (c) x = 6. Scan rate: 100 mV s^{-1}. Black curves - under argon, red curves - under CO_2. Pt disc microelectrode.

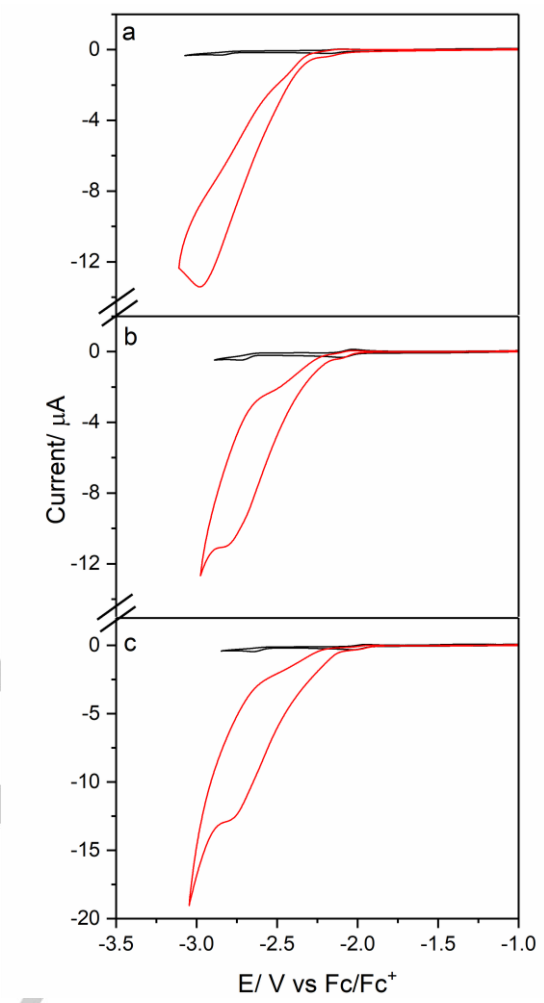

Figure 5. CV of $[Mo(CO)_4(x,x'\text{-dmbipy})]$ in CO_2-saturated NMP/Bu_4NPF_6. (a) x = 4. (b) x = 5. (c) x = 6. Scan rate: 100 mV s^{-1}. Black curves - under argon, red curves - under CO_2. Au disc microelectrode.

In CO_2-saturated NMP, the catalytic performance at a platinum disc microelectrode (Figure 4) is comparable with that observed in THF, involving dominantly the high-overpotential pathway at R2. The slight enhancement in NMP can be ascribed to the ability of the 2e-reduced bipy ligand to act as a parking station for H^+, facilitating the catalytic action.[49]

Reducing $[Mo(CO)_4(x,x'\text{-dmbipy})]$ at the gold disc microelectrode in CO_2-saturated NMP (Figure 5) has a remarkably strong synergetic effect, with the catalytic current exceeding more than three times the maximum values passed at the platinum disc microelectrode under the same conditions (Figure 4). Moreover, the onset of the electrocatalytic process coincides with the cathodic wave R2' seen under argon (Figure S3). These experimental conditions offer the best performance but are also serving to illustrate the apparent sensitivity of the low-overpotential ECE pathway to solvent changes.

Infrared spectroelectrochemistry and thin-layer cyclic voltammetry largely confirm the major observations made on the subsecond time scale of conventional CV. In argon-saturated dry THF, the reduction of parent $[Mo(CO)_4(x,x'\text{-dmbipy})]$ to $[Mo(CO)_4(x,x'\text{-dmbipy})]^{\bullet-}$ at R1 is accompanied by a low-energy shift of the four v(CO) absorption bands (Table 2, Figure 6a). For the second reduction at R2 the magnitude of the v(CO) shift is almost doubled and the fingerprint band pattern adopts a tricarbonyl form, confirming the presence of a strongly π-delocalized[49] 5-coordinate dianion, $[Mo(CO)_3(x,x'\text{-dmbipy})]^{2-}$. This characteristic behavior was also encountered for the remaining two studied complexes (Table 2).

The characteristic low-energy v(CO) shift accompanying the formation of the stable radical anions $[Mo(CO)_4(x,x'\text{-dmbipy})]^{\bullet-}$ is seen also in NMP in the course of the reduction at R1 (Table 2, Figure 6b). The v(CO) values for the parent tetracarbonyls and the corresponding radical anions are smaller in NMP by a few wavenumbers compared to THF, and the shift magnitudes, Δv(CO), upon the one-electron reduction are slightly higher in the

Table 2. Infrared and UV-vis absorption data for $[Mo(CO)_4(x,x'\text{-dmbipy})]$ (x = 4-6) and their reduction products in THF, unless otherwise stated.

Complex	ν(CO)/ cm^{-1}	λ_{max}/ nm
$[Mo(CO)_4(bipy)]$	2012, 1900, 1882, 1940	258, 297, 393, 462
$[Mo(CO)_4(4,4'\text{-dmbipy})]$	2011, 1898, 1877, 1837	259, 293, 402, 453
$[Mo(CO)_4(4,4'\text{-dmbipy})]$ [a]	2009, 1895, 1873, 1832	259, 294, 402, 440
$[Mo(CO)_4(5,5'\text{-dmbipy})]$	2011, 1899, 1879, 1839	-[b]
$[Mo(CO)_4(5,5'\text{-dmbipy})]$[a]	2010, 1897, 1875, 1833	-[b]
$[Mo(CO)_4(6,6'\text{-dmbipy})]$	2014, 1900, 1879, 1836	-[b]
$[Mo(CO)_4(6,6'\text{-dmbipy})]$ [a]	2013, 1898, 1874, 1829	-[b]
$[Mo(CO)_4(bipy)]^{\bullet-}$	1991, 1871, 1843, 1805	260, 306, 366, 463, 491, 532, <700
$[Mo(CO)_4(4,4'\text{-dmbipy})]^{\bullet-}$	1991, 1869, 1841, 1802	266, 311, 370, 472, 509, 545, <700
$[Mo(CO)_4(4,4'\text{-dmbipy})]^{\bullet-}$[a]	1989, 1867, 1841, 1800	266, 311, 369, 470, 510, 545, <700
$[Mo(CO)_4(5,5'\text{-dmbipy})]^{\bullet-}$	1989, 1868, 1840, 1800	-[b]
$[Mo(CO)_4(5,5'\text{-dmbipy})]^{\bullet-}$[a]	1988, 1865, 1839, 1798	-[b]
$[Mo(CO)_4(6,6'\text{-dmbipy})]^{\bullet-}$	1994, 1873, 1844, 1801	-[b]
$[Mo(CO)_4(6,6'\text{-dmbipy})]^{\bullet-}$[a]	1992, 1869, 1842, 1797	-[b]
$[Mo(CO)_4(bipy\text{-}H)]^-$	1994, 1874, 1848, 1807	265, 304, 396, 509
$[Mo(CO)_4(4,4'\text{-dmbipy-}H)]^-$[a]	1994, 1871, 1845, 1802	266, 309, 398, 522
$[Mo(CO)_4(5,5'\text{-dmbipy-}H)]^-$[a]	1995, 1872, 1847, 1803	-[b]
$[Mo(CO)_4(6,6'\text{-dmbipy-}H)]^-$[a]	1996, 1874, 1845, 1798	-[b]
$[Mo(CO)_3(bipy)]^{2-}$	1846, 1725, 1706	258, 369, 550sh, 580, 644
$[Mo(CO)_3(4,4'\text{-dmbipy})]^{2-}$	1841, 1712, 1699	264, 327, 421, 446, 543
$[Mo(CO)_3(5,5'\text{-dmbipy})]^{2-}$	1840, 1721, 1703	-[b]
$[Mo(CO)_3(6,6'\text{-dmbipy})]^{2-}$	1845, 1718	-[b]

[a]These values were recorded in NMP. [b] Not measured.

latter solvent. However, the major product of the second cathodic step at R2 in NMP is not the tricarbonyl 5-coordinate dianion seen in THF, but another two-electron-reduced (diamagnetic) complex with the preserved parent cis tetracarbonyl ν(CO) band pattern and wavenumbers slightly larger than those recorded for the singly reduced radical anion (Table 2, Figure 6b).

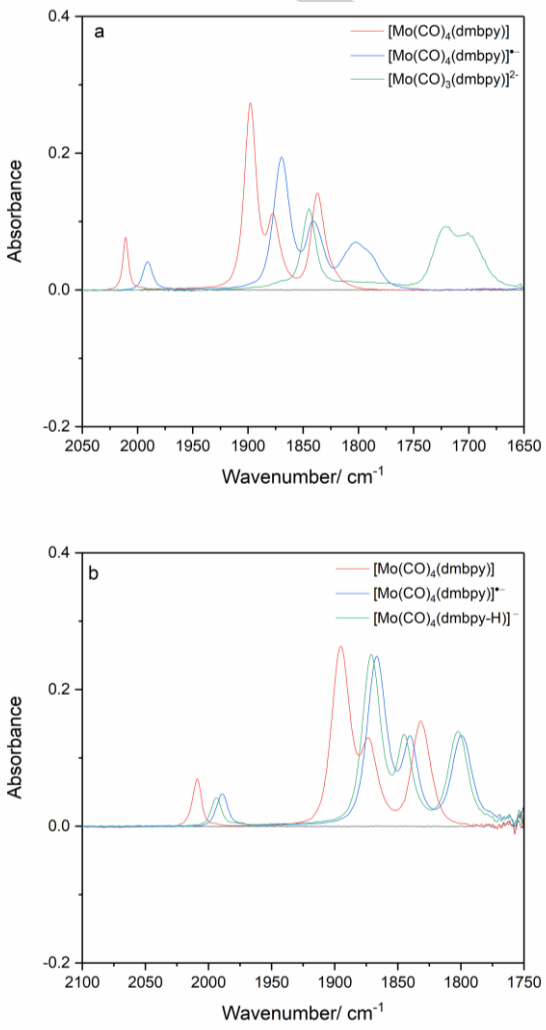

Figure 6. a) IR SEC monitoring of $[Mo(CO)_4(4,4'\text{-dmbipy})]$ in THF/Bu_4NPF_6 showing conversion from the parent (red) to its radical anion (blue) and finally to five-coordinate $[Mo(CO)_3(4,4'\text{-dmbipy})]^{2-}$, identified as the active CO_2 catalyst (green). b) IR SEC monitoring of $[Mo(CO)_4(4,4'\text{-dmbipy})]$ in NMP/Bu_4NPF_6 showing conversion of the parent (red) to its radical anion (blue) and then to $[Mo(CO)_4(4,4'\text{-dmbipy-}H)]^-$ (green**).**

UV-vis spectral monitoring of the one-electron reduction of $[Mo(CO)_4(4,4'\text{-dmbipy})]$ in THF (Figure S6(a)) and NMP (Figure S6(b) revealed in both solvents the broad π*π* intraligand electronic absorption in the low-energy visible and NIR region characteristic for the 4,4'-dmbipy radical anion (Table 2). The electronic absorption spectrum of the two-electron-reduced species produced in NMP (Figure S6(b)) further distinguishes it from $[Mo(CO)_3(4,4'\text{-dmbipy})]^{2-}$ (Figure S6(a), showing an intense absorption at λ_{max} = 398 nm that points to the presence of a coordinated 2,2'-bipyridine anion. These observations and a thorough comparison with the cathodic path of $[Mo(CO)_4(bipy)]$ (ref.[49]) lead to the assignment of the dominant ultimate two-electron reduction product in NMP as the protonated anionic complex, $[Mo(CO)_4(4,4'\text{-dmbipy-}H)]^-$. The dimethyl substitution at

the bipy skeleton and the comparable ν(CO) wavenumbers (Table 2) point to the likely protonation of the donor nitrogen atom(s).

The stabilized protonated anionic complexes $[Mo(CO)_4(x,x'\text{-dmbipy-H})]^-$ formed in NMP (still with some water content) are oxidized much less negatively than the parent complexes $[Mo(CO)_4(x,x'\text{-dmbipy})]$ are reduced. The oxidation potentials reach ca. -1.15 V at a platinum microelectrode (Figure S2) and ca. -1.30 V at a gold microelectrode. Oxidation of $[Mo(CO)_4(4,4'\text{-dmbipy-H})]^-$ was shown with thin-layer cyclic voltammetry and IR SEC to directly recover $[Mo(CO)_4(4,4'\text{-dmbipy})]$ (Figure S7). It is notable that the formation of $[Mo(CO)_4(4,4'\text{-dmbipy-H})]^-$ is not seen in NMP saturated with CO_2.

The catalytic activity of the $2e^-$-reduced complexes towards carbon dioxide reduction was examined with IR SEC for $[Mo(CO)_4(x,x'\text{-dmbipy})]$ (x = 4 and 6). In the CO_2-saturated THF electrolyte, the initial reduction of both complexes at R1, set within an OTTLE cell at the platinum or gold minigrid working electrodes, was passed smoothly, producing the stable radical anions. Sweeping the cathodic potential in the range between R1 and R2, there was a very limited evidence for CO_2 reduction, reflected in the slightly diminished $^{13}CO_2$ satellite band at 2272 cm^{-1} and subordinate bicarbonate absorption at 1675 and 1638 cm^{-1} accompanying the formation of CO. This observation is fully consistent with the conventional CV responses in Figures 2 and 3. Reaching the negative potential of R2, the $^{13}CO_2$ satellite peak drops rapidly. The complex $[Mo(CO)_4(6,6'\text{-dmbipy})]$ is more active at the gold cathode (Figure S8), with an evidence for the formation of formate (1605 cm^{-1}), suggesting some selectivity in the catalyst performance at different cathodic surfaces.

Strong enhancement of the catalytic CO_2 reduction resulting from the synergy between NMP and the gold cathodic surface is apparent also from the IR spectroelectrochemical monitoring of the ECE cathodic path dominating under these conditions (Figures S8 for the tetracarbonyl 4,4'-dmbipy complex and S9 for the 6,6'-dmbipy complex). In both cases the efficient generation of free CO adsorbed onto the cathodic surface is perceptible as a characteristic weak absorption band at 2133 (Pt) and 2130 (Au) cm^{-1} (Figures S9 and S10). The strong NMP absorption below 1700 cm^{-1} prevents to detect any carbonyl side products. At Au, the catalytic efficiency is highest, as evidenced by the faster decay of the $^{13}CO_2$ satellite band at 2272 cm^{-1}. For both the 4,4'-dmbipy and 6,6'-dmbipy complexes the catalytic CO_2 reduction on Au is triggered just after the conversion of the parent to its radical anion, at the cathodic potential of the experimentally observed R2' wave (Figure S3).

Conclusions

We have shown that the judicious placement of the substituent methyl groups at the 2,2'-bipyridine ligand in $[Mo(CO)_4(x,x'\text{-dmbipy})]$ can alter the reductive pathway leading to the two-electron-reduced catalysts of the CO_2 reduction to CO, $[Mo(CO)_3(x,x'\text{-dmbipy})]^{2-}$. In THF, the substitution in the 4,4'- and 5,5'-positions favours the high-energy EEC pathway, while with the substitution in the 6,6'-positions the low-energy ECE pathway becomes dominant, involving perceptible CO dissociation from the primary radical anion. The positive response of the catalyst to the NMP solvent compared to THF is remarkable, promoting the CO-dissociation to a such a degree that the low-overpotential pathway becomes dominant for the whole x,x'-dmbipy series. In general, the solvent and electrode effects on the catalytic performance apparently play a stronger role than the substituents in determining the catalytic pathway; although, the latter also need to be considered. Promisingly, for 6,6'-dmbipy, there is a clear enhancement of the catalytic activity relative to unsubstituted $[Mo(CO)_4(bipy)]$ in both THF (Figures S4 and S5, compare with Figures 3c and 7c) and NMP (ref.[49]). The Group-6 complexes formed by the tetracarbonyl moiety chelated by α-diimine ligands remain a promising family of electrocatalysts suited for CO_2 conversion that deserve more attention. Our ongoing studies of these complexes focus on using SFG spectroscopy to gain more insight to the cathodic surface dynamics that obviously plays a key role in these electrocatalytic processes.

Experimental Section

Materials and Methods sections can be found in the ESI. The studied complexes were synthesised according to slightly modified established literature procedures. $[Mo(CO)_6]$ and the x,x'-dimethyl-2,2'-bipyridine of choice were dissolved in equimolar amounts in argon-saturated toluene (35 mL) and refluxed for roughly 4 h using standard Schlenk techniques. An orange powder precipitated and was isolated by filtration, then washed with hexane three times to yield spectroscopically pure samples. Purity confirmed by ^1H NMR and infrared spectroscopy.[61]

$[Mo(CO)_4(4,4'\text{-dimethyl-2,2'-bipyridine})]$. Bright orange powder (268.6 mg, 86.5%). FT-IR (THF, ν(CO)) 2011, 1898, 1877, 1837 cm^{-1}. 1H NMR (400 MHz, CD_2Cl_2) δ 8.82 (2H, d, *J* = 5.3 Hz), 7.87 (2H, s), 7.14 (2H, d, *J* = 4.8 Hz), 2.44 (6H, s).

$[Mo(CO)_4(5,5'\text{-dimethyl-2,2'-bipyridine})]$. Bright orange powder (338.3 mg, 79.4%). FT-IR (THF, ν(CO)) 2011, 1899, 1879, 1839 cm^{-1}. 1H NMR (400 MHz, CD_2Cl_2) δ 8.82 (2H, s), 7.90 (2H, d, *J* = 8.2 Hz), 7.66 (2H, d, *J* = 8.0 Hz), 2.35 (6H, s).

$[Mo(CO)_4(6,6'\text{-dimethyl-2,2'-bipyridine})]$. Light red powder (129.5 mg, 30%). FT-IR (THF, ν(CO)) 2014, 1900, 1879, 1836 cm^{-1}. 1H NMR (400 MHz, CD_2Cl_2) δ 7.84 (2H, d, *J* = 7.6 Hz), 7.74 (2H, t, *J* = 7.5 Hz), 7.32 (2H, d, *J* = 7.1 Hz), 2.95 (6H, s).

Acknowledgements

This work was funded jointly by EPSRC and Spectroelectrochemistry Reading, a spin-out compay of the University of Reading (F.H.).

Keywords: Molybdenum carbonyl • Dimethylbipyridine • Spectro-electrochemistry • CO_2 reduction • Redox catalysis

[1] J. Qiao, Y. Liu, F. Hong, J. Zhang, *Chem. Soc. Rev.* **2014**, *43*, 631–675.

[2] C. Costentin, M. Robert, J. M. Savéant, *Chem. Soc. Rev.* **2013**, *42*, 2423–2436.

[3] C. Finn, S. Schnittger, L. J. Yellowlees, J. B. Love, *Chem. Commun.* **2012**, *48*, 1392–1399.

[4] K. Li, X. An, K. H. Park, M. Khraisheh, J. Tang, *Catal. Today* **2014**, *224*, 3–12.

[5] E. Portenkirchner, S. Schlager, D. Apaydin, K. Oppelt, M. Himmelsbach, D. A. M. Egbe, H. Neugebauer, G. Knör, T. Yoshida, N. S. Sariciftci, *Electrocatalysis* **2015**, *6*, 185–197.

[6] A. Maurin, C.O. Ng, L. Chen, T. C. Lau, M. Robert, C. C. Ko, *Dalton Trans.* **2016**, *45*, 14524–14529.

[7] F. Franco, C. Cometto, C. Garino, C. Minero, F. Sordello, C. Nervi, R. Gobetto, *Eur. J. Inorg. Chem.* **2015**, *2015*, 296–304.

[8] J. K. Nganga, C. R. Samanamu, J. M. Tanski, C. Pacheco, C. Saucedo, V. S. Batista, K. A. Grice, M. Z. Ertem, A. M. Angeles-Boza, *Inorg. Chem.* **2017**, *56*, 3214–3226.

[9] N. P. Liyanage, H. A. Dulaney, A. J. Huckaba, J. W. Jurss, J. H. Delcamp, *Inorg. Chem.* **2016**, *55*, 6085–6094.

[10] A. Ge, B. Rudshteyn, J. Zhu, R. J. Maurer, V. S. Batista, T. Lian, *J. Phys. Chem. Lett.* **2018**, *9*, 406–412.

[11] F. H. Haghighi, H. Hadadzadeh, H. Farrokhpour, N. Serri, K. Abdi, H. Amiri Rudbari, *Dalton Trans.* **2014**, *43*, 11317.

[12] B. A. Johnson, H. Agarwala, T. A. White, E. Mijangos, S. Maji, S. Ott, *Chem. Eur. J.* **2016**, *22*, 14870–14880.

[13] T. A. White, S. Maji, S. Ott, *Dalton Trans.* **2014**, *43*, 15028–15037.

[14] Z. Chen, C. Chen, D. R. Weinberg, P. Kang, J. J. Concepcion, D. P. Harrison, M. S. Brookhart, T. J. Meyer, *Chem. Commun.* **2011**, *47*, 12607.

[15] M. Daryanavard, H. Hadadzadeh, M. Weil, H. Farrokhpour, *J. CO2 Util.* **2017**, *17*, 80–89.

[16] H. Hadadzadeh, H. Farrokhpour, J. Simpson, J. Shakeri, M. Daryanavard, M. Shokrollahi, *New J. Chem.* **2016**, *40*, 6347–6357.

[17] D. Ghosh, K. Kobayashi, T. Kajiwara, S. Kitagawa, K. Tanaka, *Inorg. Chem.* **2017**, *56*, 11066–11073.

[18] S. Min, S. Rasul, H. Li, D. C. Grills, K. Takanabe, L.-J. Li, K.-W. Huang, *Chempluschem* **2016**, *81*, 166–171.

[19] M. R. M. Bruce, E. Megehee, B. P. Sullivan, H. Thorp, T. R. O'Toole, A. Downard, T. J. Meyer, *Organometallics* **1988**, *7*, 238–240.

[20] M. R. M. Bruce, E. Megehee, B. P. Sullivan, H. H. Thorp, T. R. O'Toole, A. Downard, J. R. Pugh, T. J. Meyer, *Inorg. Chem.* **1992**, *31*, 4864–4873.

[21] J. Tory, L. King, A. Maroulis, M. Haukka, M. J. Calhorda, F. Hartl, *Inorg. Chem.* **2014**, *53*, 1382–1396.

[22] P. Paul, B. Tyagi, A. K. Bilakhiya, M. M. Bhadbhade and E. Suresh, G. Ramachandraiah, *Inorg. Chem.*, **1998**, *37*, 5733-5742.

[23] S. E. Witt, T. A. White, Z. Li, K. R. Dunbar, C. Turro, *Chem. Commun.* **2016**, *52*, 12175–12178.

[24] G. F. Manbeck, K. Garg, T. Shimoda, D. J. Szalda, M. Z. Ertem, J. T. Muckerman, E. Fujita, *Faraday Discuss.* **2017**, *198*, 301–317.

[25] A. Szymaszek, F. P. Pruchnik, *J. Organomet. Chem.* **1989**, *376*, 133–140.

[26] S. T. Ahn, E. A. Bielinski, E. M. Lane, Y. Chen, W. H. Bernskoetter, N. Hazari, G. T. R. Palmore, *Chem. Commun.* **2015**, *51*, 5947–5950.

[27] F. D. Sypaseuth, C. Matlachowski, M. Weber, M. Schwalbe, C. C. Tzschucke, *Chem. Eur. J.* **2015**, *21*, 6564–6571.

[28] M. Bourrez, F. Molton, S. Chardon-Noblat, A. Deronzier, *Angew. Chemie Int. Ed.* **2011**, *50*, 9903–9906.

[29] F. Franco, C. Cometto, L. Nencini, C. Barolo, F. Sordello, C. Minero, J. Fiedler, M. Robert, R. Gobetto, C. Nervi, *Chem. - A Eur. J.* **2017**, *23*, 4782–4793.

[30] S. J. P. Spall, T. Keane, J. Tory, D. C. Cocker, H. Adams, H. Fowler, A. J. H. M. Meijer, F. Hartl, J. A. Weinstein, *Inorg. Chem.* **2016**, *55*, 12568 - 12582.

[31] K. T. Ngo, M. McKinnon, B. Mahanti, R. Narayanan, D. C. Grills, M. Z. Ertem, J. Rochford, *J. Am. Chem. Soc.* **2017**, *139*, 2604–2618.

[32] D. C. Grills, J. A. Farrington, B. H. Layne, S. V. Lymar, B. A. Mello, J. M. Preses, J. F. Wishart, *J. Am. Chem. Soc.* **2014**, *136*, 5563–5566.

[33] Y. C. Lam, R. J. Nielsen, H. B. Gray, W. A. Goddard, *ACS Catal.* **2015**, *5*, 2521–2528.

[34] Q. Zeng, J. Tory, F. Hartl, *Organometallics* **2014**, *33*, 5002–5008.

[35] F. Franco, C. Cometto, F. Ferrero Vallana, F. Sordello, E. Priola, C. Minero, C. Nervi, R. Gobetto, *Chem. Commun.* **2014**, *50*, 14670–14673.

[36] G. K. Rao, W. Pell, I. Korobkov, D. Richeson, *Chem. Commun.* **2016**, *52*, 8010–8013.

[37] I. Azcarate, C. Costentin, M. Robert, J.-M. Savéant, *J. Am. Chem. Soc.* **2016**, *138*, 16639–16644.

[38] C. Costentin, S. Drouet, M. Robert, J.-M. Savéant, *Science* **2012**, *338*, 90–94.

[39] A. Taheri, E. J. Thompson, J. C. Fettinger, L. A. Berben, *ACS Catal.* **2015**, *5*, 7140–7151.

[40] S.-N. Pun, W.-H. Chung, K.-M. Lam, P. Guo, P.-H. Chan, K.-Y. Wong, C.-M. Che, T.-Y. Chen, S.-M. Peng, *J. Chem. Soc. Dalt. Trans.* **2002**, *0*, 575.

[41] E. A. Mohamed, Z. N. Zahran, Y. Naruta, *Chem. Commun.* **2015**, *51*, 16900–16903.

[42] Z. N. Zahran, E. A. Mohamed, Y. Naruta, *Sci. Rep.* **2016**, *6*, 24533.

[43] R. B. Ambre, Q. Daniel, T. Fan, H. Chen, B. Zhang, L. Wang, M. S. G. Ahlquist, L. Duan, L. Sun, *Chem. Commun.* **2016**, *52*, 14478–14481.

[44] M. Hammouche, D. Lexa, M. Momenteau, J. M. Saveant, *J. Am. Chem. Soc.* **1991**, *113*, 8455–8466.

[45] C. Costentin, G. Passard, M. Robert, J.-M. Savéant, *J. Am. Chem. Soc.* **2014**, *136*, 11821–11829.

[46] S. Roy, B. Sharma, J. Pécaut, P. Simon, M. Fontecave, P. D. Tran, E. Derat, V. Artero, *J. Am. Chem. Soc.* **2017**, *139*, 3685–3696.

[47] N. Elgrishi, M. B. Chambers, M. Fontecave, *Chem. Sci.* **2015**, *6*, 2522–2531.

[48] D. C. Lacy, C. C. L. McCrory, J. C. Peters, *Inorg. Chem.* **2014**, *53*, 4980–4988.

[49] J. Tory, B. Setterfield-Price, R. A. W. Dryfe, F. Hartl, *ChemElectroChem* **2015**, *2*, 213–217.

[50] F. Franco, C. Cometto, F. Sordello, C. Minero, L. Nencini, J. Fiedler, R. Gobetto, C. Nervi, *ChemElectroChem* **2015**, *2*, 1372–1379.

[51] M. L. Clark, K. A. Grice, C. E. Moore, A. L. Rheingold, C. P. Kubiak, *Chem. Sci.* **2014**, *5*, 1894–1900.

[52] D. Sieh, D. C. Lacy, J. C. Peters, C. P. Kubiak, *Chem. - A Eur. J.* **2015**, *21*, 8497–8503.

[53] N. Elgrishi, M. B. Chambers, X. Wang, M. Fontecave, *Chem. Soc.*

Rev. **2017**, *46*, 761-796.

[54] R. Francke, B. Schille, M. Roemelt, *Chem. Rev.* **2018**, *118*, 4631-4701.

[55] J. Hawecker, J.-M. Lehn, R. Ziessel, *J. Chem. Soc. Chem. Commun.* **1984**, *984*, 328.

[56] J. Tory, G. Gobaille-Shaw, A. M. Chippindale, F. Hartl, *J. Organomet. Chem.* **2014**, *760*, 30–41.

[57] D. E. Ryan, D. J. Cardin, F. Hartl, *Coord. Chem. Rev.* **2017**, *335*, 103–149.

[58] G. Neri, P. M. Donaldson, A. J. Cowan, *J. Am. Chem. Soc.* **2017**, *139*, 13791–13797.

[59] S. A. Chabolla, E. A. Dellamary, C. W. Machan, F. A. Tezcan, C. P. Kubiak, *Inorg. Chim. Acta* **2014**, *422*, 109–113.

[60] F. Hartl, P. Rosa, L. Ricard, P. Le Floch, S. Záliš, *Coord. Chem. Rev.* **2007**, *251*, 557–576.

[61] P. N. W. Baxter, J. A. Connor, **1995**, *486*, 115–121.

WILEY-VCH

Entry for the Table of Contents (Please choose one layout)

Layout 1:

COMMUNICATION

Text for Table of Contents

((Insert TOC Graphic here))

*Author(s), Corresponding Author(s)**

Page No. – Page No.

Title

Layout 2:

COMMUNICATION

Text for Table of Contents: Complexes $[Mo(CO)_4(x,x'\text{-dmbipy})]$ (x = 4-6) have all demonstrated efficient electrocatalytic reduction of CO_2 to CO. The position of the methyl substituents either directs the catalyst toward a high-energy EEC or a low-energy ECE pathways; the latter is also promoted by the synergy of the gold cathodic surface and the *N*-methyl-2-pyrrolidone (NMP) solvent compared to Pt and THF.

*James O. Taylor, Roisín D. Leavey, František Hartl**

Page No. – Page No.

Title: Solvent and Ligand Substitution Effects on Electrocatalytic Reduction of CO_2 with $[Mo(CO)_4(x,x'\text{-dimethyl-2,2′-bipyridine})]$ (x = 4-6) Enhanced at a Gold Cathodic Surface